Suche nach Elektroweakinos mit dem ATLAS Detektor

Ludwig-Maximilians-Universität München
Fakultät für Physik

Dissertation

Eric Schanet

March 2021

Supervisor: PD Dr. Jeanette Lorenz

Part I

Fundamental concepts

Part II

The 1-lepton analysis

Chapter 5

Signal region optimisation

In order to discover the rare signals predicted by the Supersymmetry (SUSY) models considered, dedicated kinematic regions enriched in signal events, so called signal region (SR) are constructed. They are optimised to be able to discover a maximum number of the signal models considered in the analysis. In this chapter, the SR optimisation procedures leading to the final SRs are introduced and discussed.

5.1 Optimisation methods

All optimisation methods used in the following need a figure of merit that should be maximised in order to define the best performing setup. While the multidimensional cut scan in section 5.1.1 and the N-1 plots approach in section 5.1.2 use the binomial discovery significance Z_{B} introduced in section 3.5, the fit scan procedure in section 5.1.3 aims to maximise the area of the expected exclusion contour.

5.1.1 Multidimensional cut scan

The first optimisation method used for designing the SRs is an N-dimensional cut scan using N observables. For each unique combination of requirements on the set of considered observables, the expected signal and background rate as well as the statistical uncertainty on the background rate is determined from the Monte Carlo (MC) samples. As this takes a non-negligible amount of time, it is crucial to restrict the amount of cut combinations. By comparing with distributions at preselection level as e.g. shown in fig. 4.3, a set of discrete cuts can be defined for each observable. In practice, a total number of $\mathcal{O}(10^7 - 10^8)$ cut combinations can still be tested on a single machine with a reasonable turnaround time.

After determining the excepted event rates and statistical uncertainties, the different cut combinations are binned into a predefined number of signal efficiency bins. For each bin, the background rejection is subsequently maximised, i.e. the cut combination with the highest background is chosen as a candidate combination for the respective signal efficiency bin. Cut combination candidates maximising the background rejection are assumed to also maximise the discovery significance. With the significance definition used herein, this is in general a valid

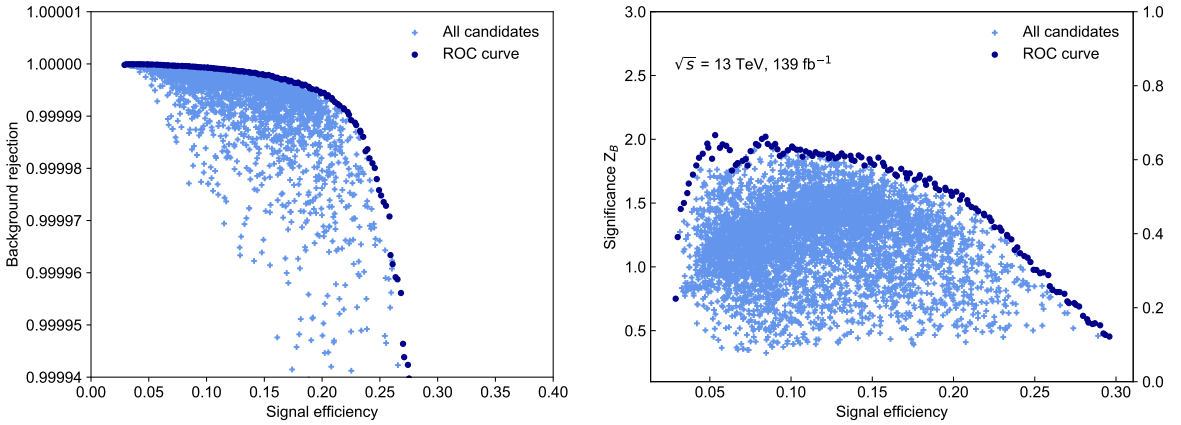

(a) **(b)**

Figure 5.1: Small N-dimensional cut scan using 10^4 unique cut combinations, illustrating the approach of (a) generating a ROC curve from the scanned cut combinations in order to (b) reduce the number of candidates used in computationally expensive significance calculations. In (b), the significance Z_B includes the MC statistical uncertainty on the expected background rate.

assumption is it tends to monotonically increase with decreasing background rate, even when the statistical uncertainty on the background estimation increases due to tighter requirements and less available MC statistics. This procedure effectively generates a receiver operating characteristic (ROC) curve. As only a small subset of all tested cut combinations are selected as candidates and lie on the ROC curve, more computationally intensive calculations can be performed, as e.g. calculating the discovery significance. This is illustrated in a small scan using 10^4 cut combinations in fig. 5.1.

A common problem of N-dimensional scans is the concept of *overtightening* the selections given the available MC statistics. Since the cross sections of the considered SUSY process are many orders of magnitude smaller than those of most of the Standard Model of Particle Physics (SM) processes, it is necessary to apply tight requirements on the kinematic observables in order to achieve a significant signal-to-background separation. However, due to the finite amount of MC statistics available, many of the more extreme cut combinations select kinematic regions where not enough MC statistics are available for a reasonable estimation of the background rates. Thus, by maximising the background rejection, it may occur that cut combinations are selected where the mere lack of MC statistics to properly estimate the background rates causes a high significance value. As the significance values obtained for such configurations are naturally not trustworthy, they need to be avoided.

In the N-dimensional cut scan implementation used herein, the available MC datasets are split in two statistically independent, equally sized subsets. This allows to compute two independent values for the discovery significance for each cut combination candidate, as well as having two ROC curves for each scan. A large difference in either the significance values or the ROC curves then is a clear indication that too tight cuts are applied for the available MC statistics. In addition, requirements on the minimum number of raw MC events for different background processes, as well as the maximum allowed statistical uncertainty on a given process, are applied. In the following, the N-dimensional cut scan implementation provided by `ahoi` [221] is used.

5.1.2 N-1 plots

Instead of performing a brute-force scan of a large set of cut combinations, a more manual approach, using repeated one-dimensional scans can be employed. In so-called $N-1$ plots, the variable distributions of the background components as well as exemplary signal processes are plotted together with the significance achieved by applying a cut on each value on the x-axis of the plotted distribution. All other selection cuts except the one on the plotted variable are applied. This allows to investigate the impact that a cut on a single observable has on the overall significance value. By repeating this process for each variable considered, it is possible to iteratively approach a cut combination yielding results comparable to a brute-force cut scan. Especially when considering a sizeable set of variables, this manual approach quickly becomes very cumbersome and runs into the risk of missing optimal cut combinations an N-dimensional cut scan would have found.

For this reason, $N-1$ plots are used in the following to verify and fine-tune the results from N-dimensional cut scans.

5.1.3 Fit scans

The last of the optimisation methods used in the following relies on simplified fit setups in order to compute the expected exclusion limits for various signal region candidates obtained using the previous methods. The simplified fit setups estimate the background contribution purely from MC and considers a systematic uncertainty on the background estimate of 30%, correlated over all signal region bins. Statistical uncertainties on the background estimation from the limited MC statistics are included for each bin. Similar to the previous methods, many different configurations can be tested, aiming to maximise the size of the expected exclusion contour.

Although being a very simple fit configuration, the statistical inference can take a significant amount of computation time. In order to keep the number of configurations to be tested at a manageable level, the signal region candidates obtained from the previous methods are only varied to a limited degree, assuming that they were already close to optimal in terms of expected exclusion area.

5.2 Optimisation procedure

The optimisation of the SRs uses experience from past analyses investigating the same signal model in the same final state [150, 151], all the while exploring new observables and SR configurations optimised for the full Run 2 dataset.

5.2.1 Benchmark signal points

A total of six so-called *benchmark* signal points representative for the entire signal grid are chosen for the first step of the optimisation procedure involving N-dimensional cut scans and

Table 5.1: List of observables and cut ranges used in the N-dimensional cut scan. All cut ranges, except for N_{jet} and $N_{b-\text{jet}}$, are allowed not to be applied at all.

Observable		Cut values
$E_{\text{T}}^{\text{miss}}$ [GeV]	$>$	$\in \{200, 220, 240, 260, 280, 300, 320, 340\}$
$E_{\text{T}}^{\text{miss}}$ significance	$>$	$\in \{5, 10, 15\}$
m_{T} [GeV]	$>$	$\in \{100, 120, 140, 160, 180, 200, 220, 240, 260, 280, 300\}$
m_{CT} [GeV]	$>$	$\in \{100, 120, 140, 160, 180, 200, 220, 240, 260, 280, 300\}$
m_{bb} lower [GeV]	$>$	$\in \{85, 90, 95, 100, 105, 110, 115\}$
m_{bb} upper [GeV]	$<$	$\in \{130, 135, 140, 145, 150\}$
p_{T}^{ℓ} [GeV]	$>$	$\in \{20, 40, 60, 80\}$
$p_{\text{T}}^{\text{jet1}}$ [GeV]	$>$	$\in \{50, 100, 150\}$
$p_{\text{T}}^{\text{jet2}}$ [GeV]	$>$	$\in \{50, 75, 100\}$
ΔR_{jj}	$<$	$\in \{0.8, 1.0, 1.2, 2.0\}$
ΔR_{bb}	$<$	$\in \{0.8, 1.0, 1.2, 2.0\}$
N_{jet}	$\leq$	$\in \{2, 3, 4\}$
$\Delta\phi(\boldsymbol{E}_{\text{T}}^{\text{miss}}, \boldsymbol{p}_{\text{T}}^{\ell})$ [rad]	$>$	$\in \{0.5, 1.0, 2.0, 2.5\}$

$N-1$ plots. Apart from the variables introduced in section 4.6, a set of additional, potentially discriminative observables are considered in the N-dimensional cut scan[†]:

- Transverse momenta of the two leading jets as well as the lepton. Especially for signal models with high mass differences between the $\tilde{\chi}_1^{\pm}/\tilde{\chi}_2^0$ and the $\tilde{\chi}_1^0$, the transverse momenta of the lepton and the jets tend to be higher than in background processes.
- Object-based $E_{\text{T}}^{\text{miss}}$ significance S [222], a quantity designed to offer good discrimination against fake $E_{\text{T}}^{\text{miss}}$ caused by mismeasurements or the non-hermeticity of the detector. Events with a large share of fake $E_{\text{T}}^{\text{miss}}$ accumulate at low values of S, while events with mostly real $E_{\text{T}}^{\text{miss}}$ tend to have large values of S.
- The distance between the two leading jets ΔR_{jj} as well as the two b-jets ΔR_{bb}. As the two b-jets originating from the Higgs decay in the signal scenario tend to be close together and the highest-p_{T} jets in an event, both ΔR_{jj} and ΔR_{bb} tend to have small values for signal events. In background processes, the two leading (b-)jets often do not originate from the same object and thus tend to be further apart.
- The azimuthal distance between the lepton p_{T} and the missing transverse momentum, $\Delta\phi(\boldsymbol{p}_{\text{T}}^{\ell}, \boldsymbol{p}_{\text{T}}^{\text{miss}})$. This observable exploits the fact that the lepton and the $E_{\text{T}}^{\text{miss}}$ tend to have a more back-to-back configuration in signal events than in many background processes where the lepton and the neutrino (often responsible for most of the $E_{\text{T}}^{\text{miss}}$ in an event) often originate from the same W boson.

In order to avoid selecting cut combination candidates with overtightened selection criteria compared to the available MC statistics, constraints on the relative statistical uncertainty on the background and on the raw number of MC events passing the cut combination candidates are applied. Cut combinations are only considered if they result in less than 50% relative

[†] These variables will turn out not to be used for the final signal regions and are only introduced here for completeness of the optimisation procedure description.

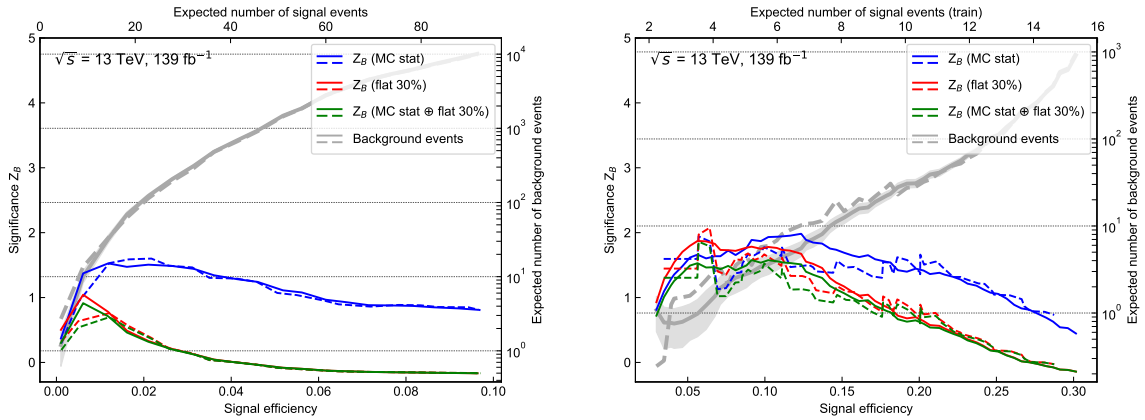

(a) **(b)**

Figure 5.2: Results of the N-dimensional cut scan for two exemplary benchmark points. The binomial discovery significance Z_{B} is plotted against the signal efficiency for varying uncertainty configurations. Additionally, the expected SM background rates are shown, including statistical uncertainty for one of the two statistically independent samples (shaded area). The solid and dashed lines represent the two statistically independent subset that the MC samples are split into.

statistical uncertainty on the total background. In addition, all cut combinations need to result in at least 5 raw MC events for each of the major backgrounds, $t\bar{t}$, single top and W + jets.

The discrete selection possibilities for each of the observables are shown in table 5.1. A preselection of one lepton and exactly two b-jets (and thus at least two jets overall in the event) is always applied. Requirements on the different observables in table 5.1 are optional and do not need to be applied by the optimisation algorithm. The results of the brute-force N-dimensional cut scans for each benchmark signal point can be visualised by plotting the expected discovery significance Z_{B} against the signal efficiency. Figure 5.2 shows the cut scan results for two of the benchmark signal points, the corresponding plots for the remaining benchmark points can be found in fig. A.1. In these figures, the binomial significance is calculated for different uncertainty configurations for each of the two statistically independent subsets. In addition, the expected background rate is shown for each of the two sample subsets. As such, these figures allow to pick a cut combination with high achieved significance while avoiding statistical fluctuations and overtightening. The cut combinations chosen for each benchmark point, after a round of $N-1$ plots, are shown in table 5.2. The $N-1$ plots, shown in figs. A.2 to A.7, are used to validate and fine-tune the cut values obtained through the cut scan and allows to remove cuts on observables that do not contribute significantly to the achieved Z_{B} value. From the initially 12 considered observables, only six (excluding the b-jet multiplicity technically not part of the scan) are part of the chosen cut combination candidates. The remaining observables turned out not to significantly improve the sensitivity.

5.2.2 Towards the final signal regions

The optimal cut combinations obtained for the benchmark signal points, shown in table 5.2, subsequently need to be consolidated into a finite set of SRs. From table 5.2, it can easily be

Table 5.2: Optimal cut combination for each benchmark signal point obtained with a brute force cut scan and a round of N-1 plots. The significance is computed for 139 fb^{-1} with the binomial discovery significance Z_B and includes MC statistical uncertainty as well as a flat 30% systematic uncertainty.

Observable	$(300, 150)$	$(400, 200)$	$(600, 300)$	$(800, 250)$	$(800, 150)$	$(800, 0)$
$N_{b-\text{jet}}$	2	2	2	2	2	2
N_{jet}	2	2	2 – 3	2 – 3	2 – 3	2 – 3
$m_{b\bar{b}}$ [GeV]	$[105 - 135]$	$[100 - 140]$	$[100 - 140]$	$[95 - 145]$	$[95 - 145]$	$[95 - 145]$
$E_{\text{T}}^{\text{miss}}$ [GeV]	> 240	> 240	> 240	> 240	> 240	> 240
m_{CT} [GeV]	> 200	> 240	> 260	> 260	> 260	> 280
m_{T} [GeV]	> 100	> 120	> 140	> 200	> 240	> 240
$m_{\ell b_1}$ [GeV]	–	–	> 150	> 120	> 120	> 120
Z_B $[\sigma]$	0.8	1.9	2.1	1.8	2.2	2.3

seen that all benchmark points favour a baseline selection including exactly two b-jets, possibly one additional light jet, a Higgs mass window requirement of roughly $m_{b\bar{b}} \in [100, 140]$ GeV, and $E_{\text{T}}^{\text{miss}} > 240$ GeV. The requirements on m_{T}, m_{CT} and $m_{\ell b_1}$ are however not easily consolidated into a single signal region, as they vastly differ depending on the model space represented by each benchmark point.

From the normalised distributions in fig. 4.3, it can already be seen that signal points from different kinematic regimes in the parameter space would in principle prefer different requirements on all three of these observables. Designing a single signal region that is optimised for the entire parameter space is thus not possible. Instead, a more generalised configuration is chosen, defining multiple signal region bins orthogonal to each other through their requirement on m_{T} and the m_{CT}, effectively creating a two-dimensional shape fit in these observables as the different SR bins can be fit simultaneously. Such a shape-fit configuration allows to exploit the differences in shape between signal and background distributions, and is able to accommodate the varying shapes of signal points from different regions in the parameter space.

The optimal number of bins as well as values of the individual bin edges in both distributions depends on the available MC statistics and is determined using the simplified fit scans introduced in section 5.1.3. The MC statistical uncertainty as well as a systematic uncertainty of 30%, correlated over all bins, is considered in each scanned configuration. The number of bins are varied in each direction (m_{T} and m_{CT}) between two and five, each time with varying bin edge values. As configurations with more bins could benefit from the additional MC statistics resulting from looser selection criteria on the remaining variables, the previously consolidated baseline selection is also allowed to vary to some extent. Configurations with multiple orthogonal SR bins in the $E_{\text{T}}^{\text{miss}}$ or $m_{b\bar{b}}$ are also included in the scan. A subset of the investigated SR candidates are shown in fig. 5.3, only showing the nominal expected exclusion limit at 95% without uncertainty bands.

As expected already from table 5.2, the best performing configurations define multiple signal region bins in the m_{T} and m_{CT} distributions, while keeping a constant baseline selection on the remaining observables. Figure 5.4(a) shows a comparison of the expected exclusion contour for exemplary two-dimensional shape-fit configurations, using signal regions binned in (m_{T}, $E_{\text{T}}^{\text{miss}}$), ($m_{\text{T}}$, $m_{b\bar{b}}$) and (m_{T}, m_{CT}). The setup using a two-dimensional shape-fit in m_{T} and

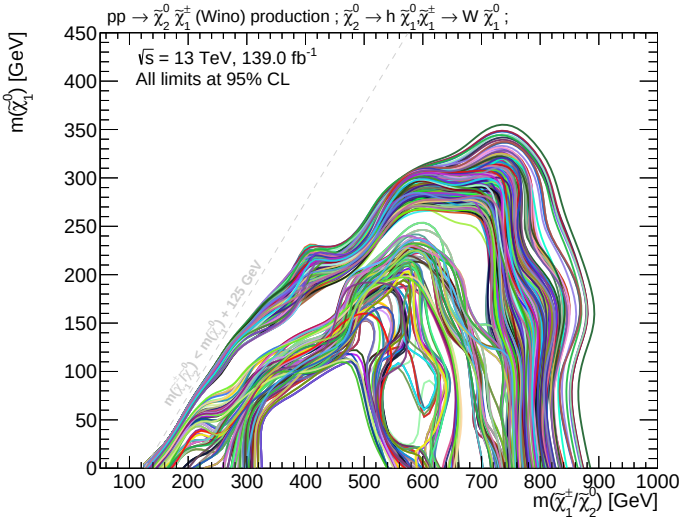

Figure 5.3: Expected exclusion contours obtained from a subset of the signal region candidates. The background estimation is taken directly from MC and includes MC statistical uncertainty as well as an uncorrelated shape uncertainty of 30%. For the sake of visibility, only the nominal contours are shown (without uncertainty bands).

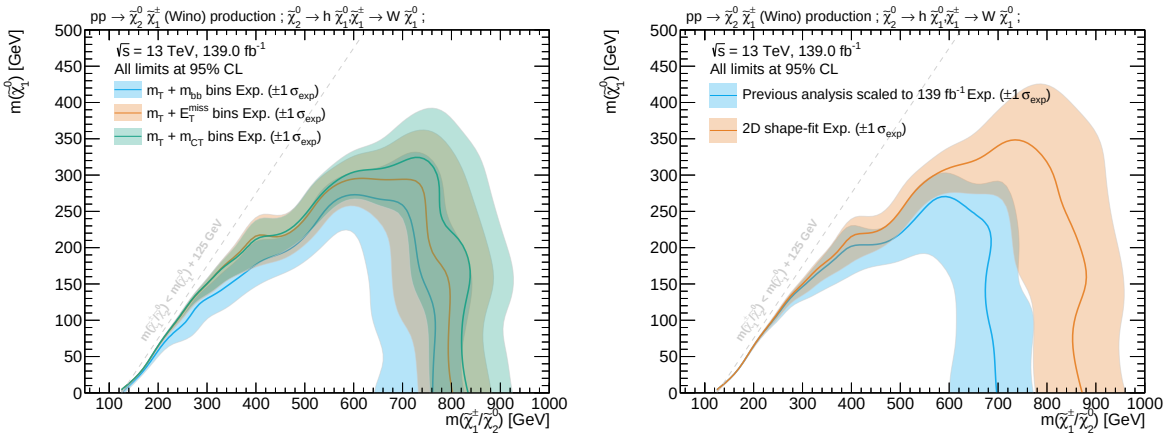

(a) **(b)**

Figure 5.4

m_{CT} clearly maximises the expected excluded area. In addition, this configuration also leads to optimal sensitivity within the expected limit, as can be seen in fig. A.8(a). Finally, applying a requirement on high values of $m_{\ell b_1}$ in the highest m_{T} bins has been shown (see fig. A.8(b)) to significantly improve sensitivity to signal models with high mass differences.

5.3 Signal region definitions

An overview of the final signal region definitions is provided in table 5.3. Based on the previously discussed results, three signal regions bins in m_{T} are defined, optimised for the low (SRLM), medium (SRMM), and high (SRHM) mass difference regimes. While SRLM targets the smallest values of m_{T}, SRMM and SRHM target progressively increasing values of m_{T}. All three signal regions are further divided into three m_{CT} bins each, resulting in a total of nine disjoint SR bins. The signal region with the highest requirement on m_{T} (SRHM) also requires $m_{\ell b_1} > 120\,\mathrm{GeV}$,

Table 5.3: Overview of the selection criteria for the signal regions. *Exclusion* SRs are defined for model-dependent limits, and *discovery* SRs are defined for model-independent limits. Each of the three exclusion SRs is binned in three m_{CT} regions for a total of nine exclusion bins.

	SRLM	**SRMM**	**SRHM**
N_{lepton}	$= 1$		
p_{T}^{ℓ} [GeV]	$> 7(6)$ for $e(\mu)$		
N_{jet}	$= 2$ or 3		
$N_{b\text{-jet}}$	$= 2$		
$E_{\mathrm{T}}^{\mathrm{miss}}$ [GeV]	> 240		
$m_{b\bar{b}}$ [GeV]	$\in [100, 140]$		
$m(\ell, b_1)$ [GeV]	–	–	> 120
m_{T} [GeV] (excl.)	$\in [100, 160]$	$\in [160, 240]$	> 240
m_{CT} [GeV] (excl.)	$\{\in [180, 230], \in [230, 280], > 280\}$		
m_{T} [GeV] (disc.)	> 100	> 160	> 240
m_{CT} [GeV] (disc.)	> 180		

for the reason explained previously. All three SRs otherwise share a common set of requirements on the number of jets, $E_{\mathrm{T}}^{\mathrm{miss}}$ and $m_{b\bar{b}}$. As shape-fits are by construction highly model-dependent[†], these SRs will be used for deriving model-dependent limits in the case where no significant excess compared to the expected SM background rate is seen in data. For this reason, the shape-fit regions will be referred to as *exclusion* regions in the following. A graphical representation of the nine exclusion signal region bins is shown in fig. 5.5.

For evaluating a potential excess in data compared to the expected background rate, a second set of signal regions is derived from the optimised shape-fit setup. For each of the three bins in the transverse mass (SRLM, SRMM, and SRHM), the three m_{CT} bins are summed up and the upper bound on m_{T} is removed (if present). This results in three cut-and-count signal regions that make minimal model assumptions and can be interpreted in any signal model as long as the predicted signal rates are known. In case of no significant excess over the SM expectation, these so-called *discovery* SRs can be used to derive model-independent limits.

[†] The signal shapes need to be known in order to estimate the expected signal rates in multiple, disjoint signal region bins.

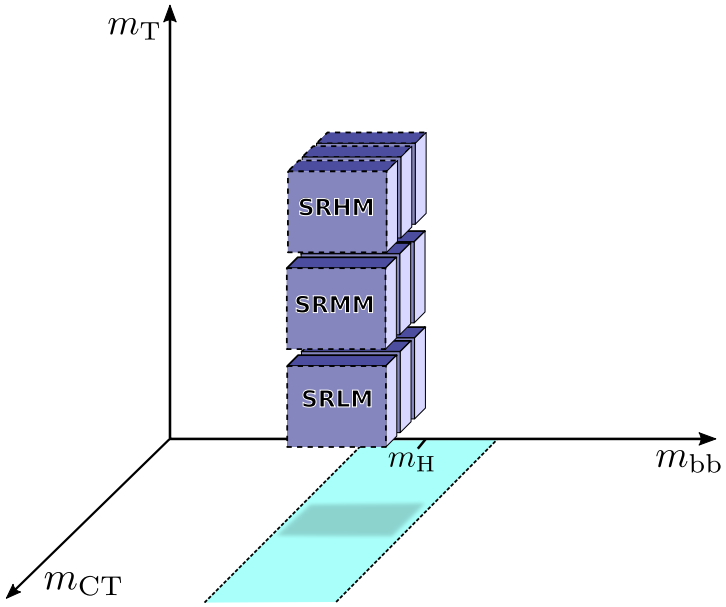

Figure 5.5: Configuration of the exclusion signal regions. Nine signal region bins are defined on m_{T} and m_{CT} within the Higgs mass window, resulting in a two-dimensional shape-fit.

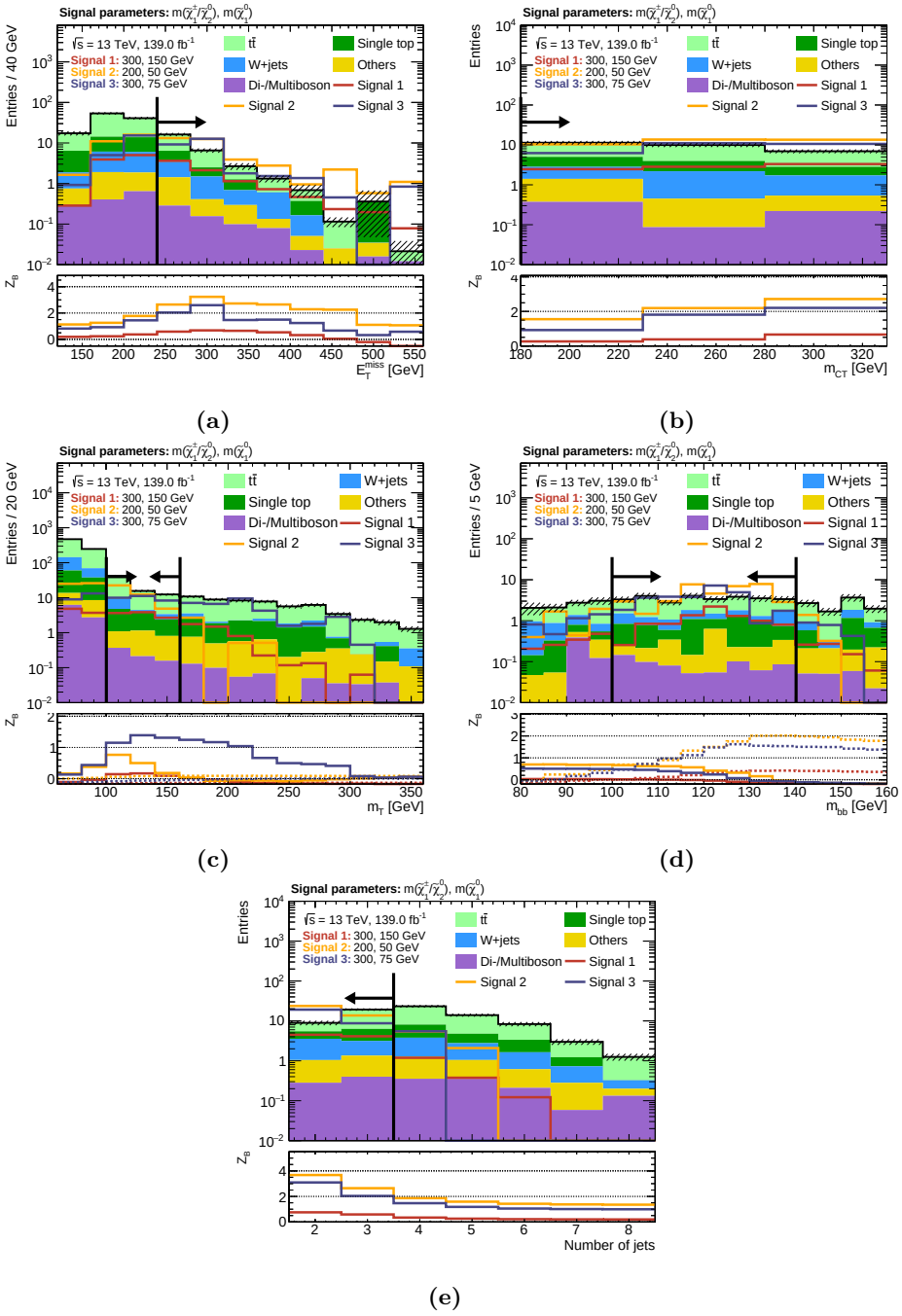

Figure 5.6: $N-1$ plots for SRLM, with exemplary signal points and all m_{CT} bins included. The dashed area represents MC statistical uncertainty on the background. In all figures except fig. (b), the significance in the lower pad is obtained by summing up all the events in the direction of the cut arrow and includes 30% uncertainty as well as MC statistical uncertainty. In fig. (b) the significance is only computed on a bin-by-bin basis, i.e. not summing up all events in the direction of the cut arrow.

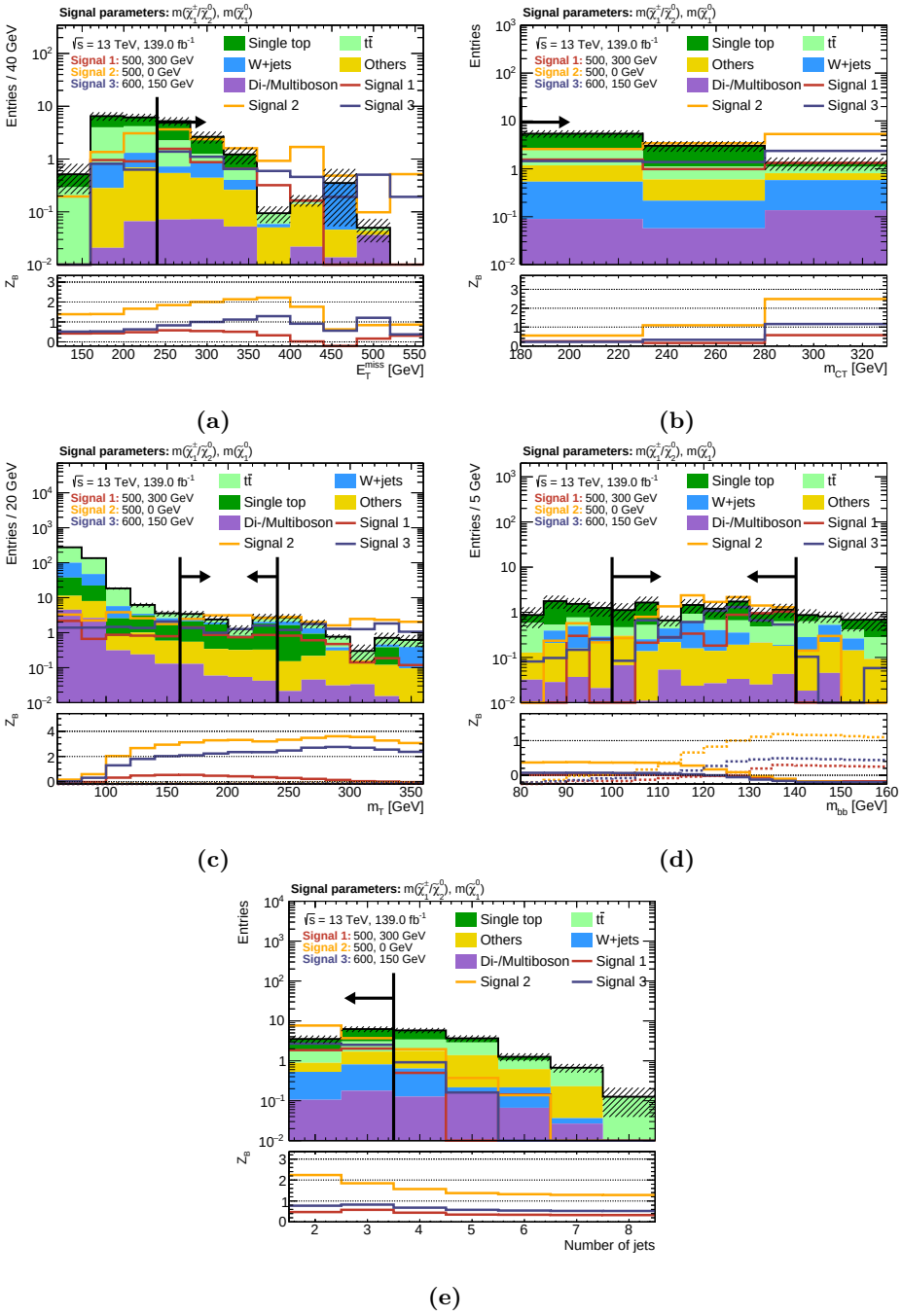

Figure 5.7: $N-1$ plots for SRMM, with exemplary signal points and all m_{CT} bins included. The dashed area represents MC statistical uncertainty on the background. In all figures except fig. (b), the significance in the lower pad is obtained by summing up all the events in the direction of the cut arrow and includes 30% uncertainty as well as MC statistical uncertainty. In fig. (b) the significance is only computed on a bin-by-bin basis, i.e. not summing up all events in the direction of the cut arrow.

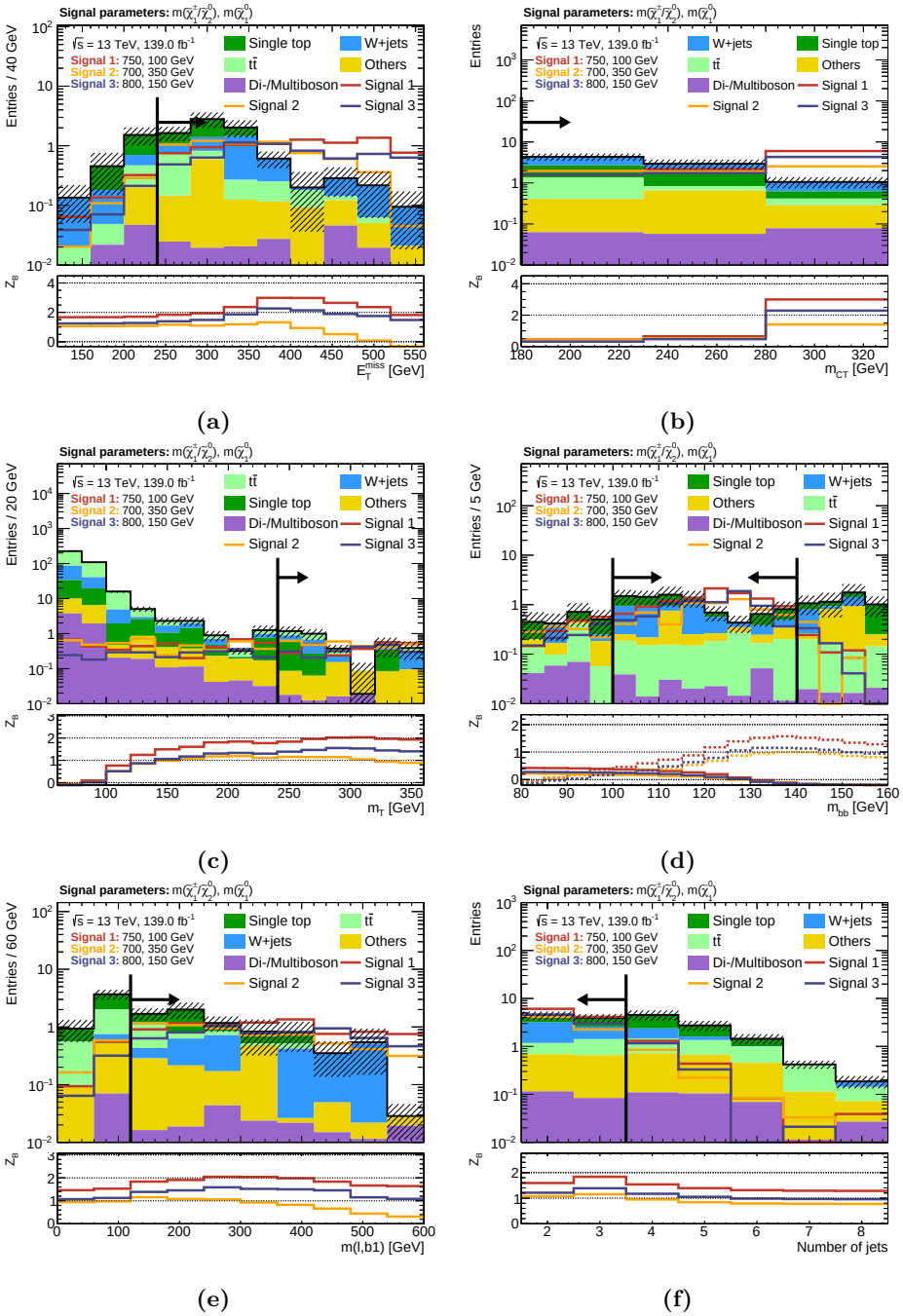

Figure 5.8: $N-1$ plots for SRHM, with exemplary signal points and all m_{CT} bins included. The dashed area represents MC statistical uncertainty on the background. In all figures except fig. (b), the significance in the lower pad is obtained by summing up all the events in the direction of the cut arrow and includes 30% uncertainty as well as MC statistical uncertainty. In fig. (b) the significance is only computed on a bin-by-bin basis, i.e. not summing up all events in the direction of the cut arrow.

Part III

Reinterpretation

Part IV

Summary and Outlook

Part V

Appendix

Abbreviations

MC Monte Carlo. 83–89, 92–94

ROC receiver operating characteristic. 84

SM Standard Model of Particle Physics. 84, 87, 90

SR signal region. 83, 85, 87–90

SUSY Supersymmetry. 83, 84

Bibliography

[1] I. C. Brock and T. Schorner-Sadenius, *Physics at the terascale*. Wiley, Weinheim, 2011. https://cds.cern.ch/record/1354959.

[2] M. E. Peskin and D. V. Schroeder, *An Introduction to quantum field theory*. Addison-Wesley, Reading, USA, 1995. http://www.slac.stanford.edu/~mpeskin/QFT.html.

[3] S. P. Martin, "A Supersymmetry primer," arXiv:hep-ph/9709356 [hep-ph]. [Adv. Ser. Direct. High Energy Phys.18,1(1998)].

[4] M. Bustamante, L. Cieri, and J. Ellis, "Beyond the Standard Model for Montaneros," in *5th CERN - Latin American School of High-Energy Physics*. 11, 2009. arXiv:0911.4409 [hep-ph].

[5] L. Brown, *The Birth of particle physics*. Cambridge University Press, Cambridge Cambridgeshire New York, 1986.

[6] P. J. Mohr, D. B. Newell, and B. N. Taylor, "CODATA Recommended Values of the Fundamental Physical Constants: 2014," *Rev. Mod. Phys.* **88** no. 3, (2016) 035009, arXiv:1507.07956 [physics.atom-ph].

[7] P. D. Group, "Review of Particle Physics," *Progress of Theoretical and Experimental Physics* **2020** no. 8, (08, 2020) , https://academic.oup.com/ptep/article-pdf/2020/8/083C01/34673722/ptaa104.pdf. https://doi.org/10.1093/ptep/ptaa104. 083C01.

[8] **Super-Kamiokande** Collaboration, Y. Fukuda *et al.*, "Evidence for oscillation of atmospheric neutrinos," *Phys. Rev. Lett.* **81** (1998) 1562–1567, arXiv:hep-ex/9807003 [hep-ex].

[9] Z. Maki, M. Nakagawa, and S. Sakata, "Remarks on the unified model of elementary particles," *Prog. Theor. Phys.* **28** (1962) 870–880. [,34(1962)].

[10] N. Cabibbo, "Unitary symmetry and leptonic decays," *Phys. Rev. Lett.* **10** (Jun, 1963) 531–533. https://link.aps.org/doi/10.1103/PhysRevLett.10.531.

[11] M. Kobayashi and T. Maskawa, "CP Violation in the Renormalizable Theory of Weak Interaction," *Prog. Theor. Phys.* **49** (1973) 652–657.

[12] E. Noether and M. A. Tavel, "Invariant variation problems," arXiv:physics/0503066.

[13] J. C. Ward, "An identity in quantum electrodynamics," *Phys. Rev.* **78** (Apr, 1950) 182–182. https://link.aps.org/doi/10.1103/PhysRev.78.182.

[14] Y. Takahashi, "On the generalized ward identity," *Il Nuovo Cimento (1955-1965)* **6** no. 2, (Aug, 1957) 371–375. https://doi.org/10.1007/BF02832514.

[15] G. 'tHooft, "Renormalization of massless yang-mills fields," *Nuclear Physics B* **33** no. 1, (1971) 173 – 199. http://www.sciencedirect.com/science/article/pii/0550321371903956.

[16] J. Taylor, "Ward identities and charge renormalization of the yang-mills field," *Nuclear Physics B* **33** no. 2, (1971) 436 – 444. http://www.sciencedirect.com/science/article/pii/0550321371902975.

[17] A. A. Slavnov, "Ward identities in gauge theories," *Theoretical and Mathematical Physics* **10** no. 2, (Feb, 1972) 99–104. https://doi.org/10.1007/BF01090719.

[18] C. N. Yang and R. L. Mills, "Conservation of isotopic spin and isotopic gauge invariance," *Phys. Rev.* **96** (Oct, 1954) 191–195. https://link.aps.org/doi/10.1103/PhysRev.96.191.

[19] K. G. Wilson, "Confinement of quarks," *Phys. Rev. D* **10** (Oct, 1974) 2445–2459. https://link.aps.org/doi/10.1103/PhysRevD.10.2445.

[20] T. DeGrand and C. DeTar, *Lattice Methods for Quantum Chromodynamics*. World Scientific, Singapore, 2006. https://cds.cern.ch/record/1055545.

[21] S. L. Glashow, "Partial-symmetries of weak interactions," *Nuclear Physics* **22** no. 4, (1961) 579 – 588. http://www.sciencedirect.com/science/article/pii/0029558261904692.

[22] S. Weinberg, "A model of leptons," *Phys. Rev. Lett.* **19** (Nov, 1967) 1264–1266. https://link.aps.org/doi/10.1103/PhysRevLett.19.1264.

[23] A. Salam and J. C. Ward, "Weak and electromagnetic interactions," *Il Nuovo Cimento (1955-1965)* **11** no. 4, (Feb, 1959) 568–577. https://doi.org/10.1007/BF02726525.

[24] C. S. Wu, E. Ambler, R. W. Hayward, D. D. Hoppes, and R. P. Hudson, "Experimental test of parity conservation in beta decay," *Phys. Rev.* **105** (Feb, 1957) 1413–1415. https://link.aps.org/doi/10.1103/PhysRev.105.1413.

[25] M. Gell-Mann, "The interpretation of the new particles as displaced charge multiplets," *Il Nuovo Cimento (1955-1965)* **4** no. 2, (Apr, 1956) 848–866. https://doi.org/10.1007/BF02748000.

[26] K. Nishijima, "Charge Independence Theory of V Particles*," *Progress of Theoretical Physics* **13** no. 3, (03, 1955) 285–304, https://academic.oup.com/ptp/article-pdf/13/3/285/5425869/13-3-285.pdf. https://doi.org/10.1143/PTP.13.285.

[27] T. Nakano and K. Nishijima, "Charge Independence for V-particles*," *Progress of Theoretical Physics* **10** no. 5, (11, 1953) 581–582, https://academic.oup.com/ptp/article-pdf/10/5/581/5364926/10-5-581.pdf. https://doi.org/10.1143/PTP.10.581.

[28] F. Englert and R. Brout, "Broken symmetry and the mass of gauge vector mesons," *Phys. Rev. Lett.* **13** (Aug, 1964) 321–323. https://link.aps.org/doi/10.1103/PhysRevLett.13.321.

[29] P. W. Higgs, "Broken symmetries and the masses of gauge bosons," *Phys. Rev. Lett.* **13** (Oct, 1964) 508–509. https://link.aps.org/doi/10.1103/PhysRevLett.13.508.

[30] P. W. Higgs, "Spontaneous symmetry breakdown without massless bosons," *Phys. Rev.* **145** (May, 1966) 1156–1163. https://link.aps.org/doi/10.1103/PhysRev.145.1156.

[31] Y. Nambu, "Quasiparticles and Gauge Invariance in the Theory of Superconductivity," *Phys. Rev.* **117** (1960) 648–663. [,132(1960)].

[32] J. Goldstone, "Field Theories with Superconductor Solutions," *Nuovo Cim.* **19** (1961) 154–164.

[33] V. Brdar, A. J. Helmboldt, S. Iwamoto, and K. Schmitz, "Type-I Seesaw as the Common Origin of Neutrino Mass, Baryon Asymmetry, and the Electroweak Scale," *Phys. Rev. D* **100** (2019) 075029, arXiv:1905.12634 [hep-ph].

[34] G. 't Hooft and M. Veltman, "Regularization and renormalization of gauge fields," *Nuclear Physics B* **44** no. 1, (1972) 189 – 213. http://www.sciencedirect.com/science/article/pii/0550321372902799.

[35] F. Zwicky, "Die Rotverschiebung von extragalaktischen Nebeln," *Helv. Phys. Acta* **6** (1933) 110–127. https://cds.cern.ch/record/437297.

[36] V. C. Rubin and W. K. Ford, Jr., "Rotation of the Andromeda Nebula from a Spectroscopic Survey of Emission Regions," *Astrophys. J.* **159** (1970) 379–403.

[37] G. Bertone, D. Hooper, and J. Silk, "Particle dark matter: Evidence, candidates and constraints," *Phys. Rept.* **405** (2005) 279–390, arXiv:hep-ph/0404175.

[38] D. Clowe, M. Bradac, A. H. Gonzalez, M. Markevitch, S. W. Randall, C. Jones, and D. Zaritsky, "A direct empirical proof of the existence of dark matter," *Astrophys. J.* **648** (2006) L109–L113, arXiv:astro-ph/0608407 [astro-ph].

[39] A. Taylor, S. Dye, T. J. Broadhurst, N. Benitez, and E. van Kampen, "Gravitational lens magnification and the mass of abell 1689," *Astrophys. J.* **501** (1998) 539, arXiv:astro-ph/9801158.

[40] C. Bennett *et al.*, "Four year COBE DMR cosmic microwave background observations: Maps and basic results," *Astrophys. J. Lett.* **464** (1996) L1–L4, arXiv:astro-ph/9601067.

[41] G. F. Smoot *et al.*, "Structure in the COBE Differential Microwave Radiometer First-Year Maps," *ApJS* **396** (September, 1992) L1.

[42] **WMAP** Collaboration, "Nine-year Wilkinson Microwave Anisotropy Probe (WMAP) Observations: Final Maps and Results," *ApJS* **208** no. 2, (October, 2013) 20, arXiv:1212.5225 [astro-ph.CO].

[43] **WMAP** Collaboration, "Nine-year Wilkinson Microwave Anisotropy Probe (WMAP) Observations: Cosmological Parameter Results," *ApJS* **208** no. 2, (October, 2013) 19, arXiv:1212.5226 [astro-ph.CO].

[44] **Planck** Collaboration, "Planck 2018 results. I. Overview and the cosmological legacy of Planck," *Astron. Astrophys.* **641** (2020) A1, arXiv:1807.06205 [astro-ph.CO].

[45] A. Liddle, *An introduction to modern cosmology; 3rd ed.* Wiley, Chichester, Mar, 2015. https://cds.cern.ch/record/1976476.

[46] **Planck** Collaboration, "Planck 2018 results. VI. Cosmological parameters," *Astron. Astrophys.* **641** (2020) A6, arXiv:1807.06209 [astro-ph.CO].

[47] H. Georgi and S. L. Glashow, "Unity of all elementary-particle forces," *Phys. Rev. Lett.* **32** (Feb, 1974) 438–441. https://link.aps.org/doi/10.1103/PhysRevLett.32.438.

[48] I. Aitchison, *Supersymmetry in Particle Physics. An Elementary Introduction*. Cambridge University Press, Cambridge, 2007.

[49] **Muon g-2** Collaboration, G. Bennett *et al.*, "Final Report of the Muon E821 Anomalous Magnetic Moment Measurement at BNL," *Phys. Rev. D* **73** (2006) 072003, arXiv:hep-ex/0602035.

[50] H. Baer and X. Tata, *Weak Scale Supersymmetry: From Superfields to Scattering Events*. Cambridge University Press, 2006.

[51] A. Czarnecki and W. J. Marciano, "The Muon anomalous magnetic moment: A Harbinger for 'new physics'," *Phys. Rev. D* **64** (2001) 013014, arXiv:hep-ph/0102122.

[52] J. L. Feng and K. T. Matchev, "Supersymmetry and the anomalous magnetic moment of the muon," *Phys. Rev. Lett.* **86** (2001) 3480–3483, arXiv:hep-ph/0102146.

[53] S. Coleman and J. Mandula, "All possible symmetries of the s matrix," *Phys. Rev.* **159** (Jul, 1967) 1251–1256. https://link.aps.org/doi/10.1103/PhysRev.159.1251.

[54] R. Haag, J. T. Lopuszanski, and M. Sohnius, "All Possible Generators of Supersymmetries of the s Matrix," *Nucl. Phys.* **B88** (1975) 257. [,257(1974)].

[55] J. Wess and B. Zumino, "Supergauge transformations in four dimensions," *Nuclear Physics B* **70** no. 1, (1974) 39 – 50. http://www.sciencedirect.com/science/article/pii/0550321374903551.

[56] H. Georgi and S. L. Glashow, "Gauge theories without anomalies," *Phys. Rev. D* **6** (Jul, 1972) 429–431. https://link.aps.org/doi/10.1103/PhysRevD.6.429.

[57] S. Dimopoulos and D. W. Sutter, "The Supersymmetric flavor problem," *Nucl. Phys. B* **452** (1995) 496–512, arXiv:hep-ph/9504415.

[58] **MEG** Collaboration, T. Mori, "Final Results of the MEG Experiment," *Nuovo Cim. C* **39** no. 4, (2017) 325, arXiv:1606.08168 [hep-ex].

[59] H. P. Nilles, "Supersymmetry, Supergravity and Particle Physics," *Phys. Rept.* **110** (1984) 1–162.

[60] A. Lahanas and D. Nanopoulos, "The road to no-scale supergravity," *Physics Reports* **145** no. 1, (1987) 1 – 139. http://www.sciencedirect.com/science/article/pii/0370157387900342.

[61] J. L. Feng, A. Rajaraman, and F. Takayama, "Superweakly interacting massive particles," *Phys. Rev. Lett.* **91** (2003) 011302, arXiv:hep-ph/0302215.

[62] **Super-Kamiokande** Collaboration, K. Abe *et al.*, "Search for proton decay via $p \to e^+\pi^0$ and $p \to \mu^+\pi^0$ in 0.31 megaton-years exposure of the Super-Kamiokande water Cherenkov detector," *Phys. Rev.* **D95** no. 1, (2017) 012004, arXiv:1610.03597 [hep-ex].

[63] J. R. Ellis, "Beyond the standard model for hill walkers," in *1998 European School of High-Energy Physics*, pp. 133–196. 8, 1998. arXiv:hep-ph/9812235.

[64] J. R. Ellis, J. Hagelin, D. V. Nanopoulos, K. A. Olive, and M. Srednicki, "Supersymmetric Relics from the Big Bang," *Nucl. Phys. B* **238** (1984) 453–476.

[65] D. O. Caldwell, R. M. Eisberg, D. M. Grumm, M. S. Witherell, B. Sadoulet, F. S. Goulding, and A. R. Smith, "Laboratory limits on galactic cold dark matter," *Phys. Rev. Lett.* **61** (Aug, 1988) 510–513. https://link.aps.org/doi/10.1103/PhysRevLett.61.510.

[66] M. Mori, M. M. Nojiri, K. S. Hirata, K. Kihara, Y. Oyama, A. Suzuki, K. Takahashi, M. Yamada, H. Takei, M. Koga, K. Miyano, H. Miyata, Y. Fukuda, T. Hayakawa, K. Inoue, T. Ishida, T. Kajita, Y. Koshio, M. Nakahata, K. Nakamura, A. Sakai, N. Sato, M. Shiozawa, J. Suzuki, Y. Suzuki, Y. Totsuka, M. Koshiba, K. Nishijima, T. Kajimura, T. Suda, A. T. Suzuki, T. Hara, Y. Nagashima, M. Takita, H. Yokoyama, A. Yoshimoto, K. Kaneyuki, Y. Takeuchi, T. Tanimori, S. Tasaka, and K. Nishikawa, "Search for neutralino dark matter heavier than the w boson at kamiokande," *Phys. Rev. D* **48** (Dec, 1993) 5505–5518. https://link.aps.org/doi/10.1103/PhysRevD.48.5505.

[67] **CDMS** Collaboration, D. S. Akerib *et al.*, "Exclusion limits on the WIMP-nucleon cross section from the first run of the Cryogenic Dark Matter Search in the Soudan Underground Laboratory," *Phys. Rev. D* **72** (2005) 052009, arXiv:astro-ph/0507190.

[68] A. Djouadi, J.-L. Kneur, and G. Moultaka, "SuSpect: A Fortran code for the supersymmetric and Higgs particle spectrum in the MSSM," *Comput. Phys. Commun.* **176** (2007) 426–455, arXiv:hep-ph/0211331.

[69] C. F. Berger, J. S. Gainer, J. L. Hewett, and T. G. Rizzo, "Supersymmetry without prejudice," *Journal of High Energy Physics* **2009** no. 02, (Feb, 2009) 023–023. http://dx.doi.org/10.1088/1126-6708/2009/02/023.

[70] J. Alwall, P. Schuster, and N. Toro, "Simplified Models for a First Characterization of New Physics at the LHC," *Phys. Rev.* **D79** (2009) 075020, arXiv:0810.3921 [hep-ph].

[71] **LHC New Physics Working Group** Collaboration, D. Alves, "Simplified Models for LHC New Physics Searches," *J. Phys.* **G39** (2012) 105005, arXiv:1105.2838 [hep-ph].

[72] D. S. Alves, E. Izaguirre, and J. G. Wacker, "Where the Sidewalk Ends: Jets and Missing Energy Search Strategies for the 7 TeV LHC," *JHEP* **10** (2011) 012, arXiv:1102.5338 [hep-ph].

[73] F. Ambrogi, S. Kraml, S. Kulkarni, U. Laa, A. Lessa, and W. Waltenberger, "On the coverage of the pMSSM by simplified model results," *Eur. Phys. J. C* **78** no. 3, (2018) 215, arXiv:1707.09036 [hep-ph].

[74] O. Buchmueller and J. Marrouche, "Universal mass limits on gluino and third-generation squarks in the context of Natural-like SUSY spectra," *Int. J. Mod. Phys. A* **29** no. 06, (2014) 1450032, arXiv:1304.2185 [hep-ph].

[75] **ATLAS** Collaboration, M. Aaboud *et al.*, "Dark matter interpretations of ATLAS searches for the electroweak production of supersymmetric particles in $\sqrt{s} = 8$ TeV proton-proton collisions," *JHEP* **09** (2016) 175, arXiv:1608.00872 [hep-ex].

[76] **ATLAS** Collaboration, "Summary of the ATLAS experiment's sensitivity to supersymmetry after LHC Run 1 — interpreted in the phenomenological MSSM," *JHEP* **10** (2015) 134, arXiv:1508.06608 [hep-ex].

[77] **ATLAS** Collaboration, "Mass reach of the atlas searches for supersymmetry." https://atlas.web.cern.ch/Atlas/GROUPS/PHYSICS/PUBNOTES/ATL-PHYS-PUB-2020-020/fig_23.png, 2020.

[78] **CMS** Collaboration, "Summary plot moriond 2017." https://twiki.cern.ch/twiki/pub/CMSPublic/SUSYSummary2017/Moriond2017_BarPlot.pdf, 2017.

[79] L. S. W. Group, "Notes lepsusywg/02-04.1 and lepsusywg/01-03.1." http://lepsusy.web.cern.ch/lepsusy/, 2004. Accessed: 2021-02-11.

[80] **ATLAS** Collaboration, G. Aad *et al.*, "Observation of a new particle in the search for the Standard Model Higgs boson with the ATLAS detector at the LHC," *Phys. Lett. B* **716** (2012) 1–29, arXiv:1207.7214 [hep-ex].

[81] **CMS** Collaboration, S. Chatrchyan *et al.*, "Observation of a New Boson at a Mass of 125 GeV with the CMS Experiment at the LHC," *Phys. Lett. B* **716** (2012) 30–61, arXiv:1207.7235 [hep-ex].

[82] CERN, "About cern." https://home.cern/about. Accessed: 2021-01-21.

[83] L. R. Evans and P. Bryant, "LHC Machine," *JINST* **3** (2008) S08001. 164 p. http://cds.cern.ch/record/1129806. This report is an abridged version of the LHC Design Report (CERN-2004-003).

[84] R. Scrivens, M. Kronberger, D. Küchler, J. Lettry, C. Mastrostefano, O. Midttun, M. O'Neil, H. Pereira, and C. Schmitzer, "Overview of the status and developments on primary ion sources at CERN*,". https://cds.cern.ch/record/1382102.

[85] E. Mobs, "The CERN accelerator complex - 2019. Complexe des accélérateurs du CERN - 2019,". https://cds.cern.ch/record/2684277. General Photo.

[86] **ATLAS** Collaboration, "The ATLAS Experiment at the CERN Large Hadron Collider," *JINST* **3** (2008) S08003.

[87] **CMS** Collaboration, S. Chatrchyan *et al.*, "The CMS Experiment at the CERN LHC," *JINST* **3** (2008) S08004.

[88] **ALICE** Collaboration, K. Aamodt *et al.*, "The ALICE experiment at the CERN LHC," *JINST* **3** (2008) S08002.

[89] **LHCb** Collaboration, J. Alves, A.Augusto *et al.*, "The LHCb Detector at the LHC," *JINST* **3** (2008) S08005.

[90] **TOTEM** Collaboration, G. Anelli *et al.*, "The TOTEM experiment at the CERN Large Hadron Collider," *JINST* **3** (2008) S08007.

[91] **LHCf** Collaboration, O. Adriani *et al.*, "Technical design report of the LHCf experiment: Measurement of photons and neutral pions in the very forward region of LHC,".

[92] **MoEDAL** Collaboration, J. Pinfold *et al.*, "Technical Design Report of the MoEDAL Experiment,".

[93] O. S. Bruning, P. Collier, P. Lebrun, S. Myers, R. Ostojic, J. Poole, and P. Proudlock, *LHC Design Report*. CERN Yellow Reports: Monographs. CERN, Geneva, 2004. https://cds.cern.ch/record/782076.

[94] **ATLAS** Collaboration, "ATLAS Public Results - Luminosity Public Results Run 2,". https://twiki.cern.ch/twiki/bin/view/AtlasPublic/LuminosityPublicResultsRun2. Accessed: 2021-01-17.

[95] **ATLAS** Collaboration, Z. Marshall, "Simulation of Pile-up in the ATLAS Experiment," *J. Phys. Conf. Ser.* **513** (2014) 022024.

[96] "First beam in the LHC - accelerating science,". https://home.cern/news/news/accelerators/record-luminosity-well-done-lhc. Accessed: 2021-01-10.

[97] **ATLAS Collaboration** Collaboration, "Luminosity determination in pp collisions at $\sqrt{s} = 13$ TeV using the ATLAS detector at the LHC," Tech. Rep. ATLAS-CONF-2019-021, CERN, Geneva, Jun, 2019. https://cds.cern.ch/record/2677054.

[98] **ATLAS** Collaboration, M. Aaboud *et al.*, "Luminosity determination in pp collisions at $\sqrt{s} = 8$ TeV using the ATLAS detector at the LHC," *Eur. Phys. J. C* **76** no. 12, (2016) 653, arXiv:1608.03953 [hep-ex].

[99] G. Avoni, M. Bruschi, G. Cabras, D. Caforio, N. Dehghanian, A. Floderus, B. Giacobbe, F. Giannuzzi, F. Giorgi, P. Grafström, V. Hedberg, F. L. Manghi, S. Meneghini, J. Pinfold, E. Richards, C. Sbarra, N. S. Cesari, A. Sbrizzi, R. Soluk, G. Ucchielli, S. Valentinetti, O. Viazlo, M. Villa, C. Vittori, R. Vuillermet, and A. Zoccoli, "The new LUCID-2 detector for luminosity measurement and monitoring in ATLAS," *Journal of Instrumentation* **13** no. 07, (Jul, 2018) P07017–P07017. https://doi.org/10.1088/1748-0221/13/07/p07017.

[100] S. van der Meer, "Calibration of the effective beam height in the ISR," Tech. Rep. CERN-ISR-PO-68-31. ISR-PO-68-31, CERN, Geneva, 1968. https://cds.cern.ch/record/296752.

[101] P. Grafström and W. Kozanecki, "Luminosity determination at proton colliders," *Progress in Particle and Nuclear Physics* **81** (2015) 97 – 148. http://www.sciencedirect.com/science/article/pii/S0146641014000878.

[102] "New schedule for CERN's accelerators and experiments,". https://home.cern/news/press-release/cern/first-beam-lhc-accelerating-science. Accessed: 2021-01-10.

[103] **ATLAS** Collaboration, G. Aad *et al.*, "Luminosity Determination in pp Collisions at $\sqrt{s} = 7$ TeV Using the ATLAS Detector at the LHC," *Eur. Phys. J. C* **71** (2011) 1630, arXiv:1101.2185 [hep-ex].

[104] **ATLAS Collaboration** Collaboration, G. Aad *et al.*, "Improved luminosity determination in pp collisions at $\sqrt{s} = 7$ TeV using the ATLAS detector at the LHC. Improved luminosity determination in pp collisions at sqrt(s) = 7 TeV using the ATLAS detector at the LHC," *Eur. Phys. J. C* **73** no. CERN-PH-EP-2013-026. CERN-PH-EP-2013-026, (Feb, 2013) 2518. 27 p. https://cds.cern.ch/record/1517411. Comments: 26 pages plus author list (39 pages total), 17 figures, 9 tables, submitted to EPJC, All figures are available at <a href=.

[105] "Record luminosity: well done LHC,". https://home.cern/news/news/accelerators/new-schedule-cerns-accelerators-and-experiments. Accessed: 2021-01-10.

[106] A. G., B. A. I., B. O., F. P., L. M., R. L., and T. L., *High-Luminosity Large Hadron Collider (HL-LHC): Technical Design Report V. 0.1*. CERN Yellow Reports: Monographs. CERN, Geneva, 2017. https://cds.cern.ch/record/2284929.

[107] J. Pequenao, "Computer generated image of the whole ATLAS detector." Mar, 2008.

[108] **ATLAS** Collaboration, "ATLAS: Detector and physics performance technical design report. Volume 1,".

[109] J. Pequenao, "Computer generated image of the ATLAS inner detector." Mar, 2008.

[110] **ATLAS Collaboration** Collaboration, K. Potamianos, "The upgraded Pixel detector and the commissioning of the Inner Detector tracking of the ATLAS experiment for Run-2 at the Large Hadron Collider," Tech. Rep. ATL-PHYS-PROC-2016-104, CERN, Geneva, Aug, 2016. https://cds.cern.ch/record/2209070. 15 pages, EPS-HEP 2015 Proceedings.

[111] **ATLAS IBL** Collaboration, B. Abbott *et al.*, "Production and Integration of the ATLAS Insertable B-Layer," *JINST* **13** no. 05, (2018) T05008, arXiv:1803.00844 [physics.ins-det].

[112] **ATLAS** Collaboration, "ATLAS Insertable B-Layer Technical Design Report," Tech. Rep. CERN-LHCC-2010-013. ATLAS-TDR-19, Sep, 2010. http://cds.cern.ch/record/1291633.

[113] **ATLAS** Collaboration, G. Aad *et al.*, "ATLAS b-jet identification performance and efficiency measurement with $t\bar{t}$ events in pp collisions at $\sqrt{s} = 13$ TeV," *Eur. Phys. J. C* **79** no. 11, (2019) 970, arXiv:1907.05120 [hep-ex].

[114] ATLAS Collaboration, "Particle Identification Performance of the ATLAS Transition Radiation Tracker." ATLAS-CONF-2011-128, 2011. https://cds.cern.ch/record/1383793.

[115] J. Pequenao, "Computer Generated image of the ATLAS calorimeter." Mar, 2008.

[116] J. Pequenao, "Computer generated image of the ATLAS Muons subsystem." Mar, 2008.

[117] S. Lee, M. Livan, and R. Wigmans, "Dual-Readout Calorimetry," *Rev. Mod. Phys.* **90** no. arXiv:1712.05494. 2, (Dec, 2017) 025002. 40 p. https://cds.cern.ch/record/2637852. 44 pages, 53 figures, accepted for publication in Review of Modern Physics.

[118] M. Leite, "Performance of the ATLAS Zero Degree Calorimeter," Tech. Rep. ATL-FWD-PROC-2013-001, CERN, Geneva, Nov, 2013. https://cds.cern.ch/record/1628749.

[119] S. Abdel Khalek *et al.*, "The ALFA Roman Pot Detectors of ATLAS," *JINST* **11** no. 11, (2016) P11013, arXiv:1609.00249 [physics.ins-det].

[120] U. Amaldi, G. Cocconi, A. Diddens, R. Dobinson, J. Dorenbosch, W. Duinker, D. Gustavson, J. Meyer, K. Potter, A. Wetherell, A. Baroncelli, and C. Bosio, "The real part of the forward proton proton scattering amplitude measured at the cern intersecting storage rings," *Physics Letters B* **66** no. 4, (1977) 390 – 394. http://www.sciencedirect.com/science/article/pii/0370269377900223.

[121] L. Adamczyk, E. Banaś, A. Brandt, M. Bruschi, S. Grinstein, J. Lange, M. Rijssenbeek, P. Sicho, R. Staszewski, T. Sykora, M. Trzebiński, J. Chwastowski, and K. Korcyl, "Technical Design Report for the ATLAS Forward Proton Detector," Tech. Rep. CERN-LHCC-2015-009. ATLAS-TDR-024, May, 2015. https://cds.cern.ch/record/2017378.

[122] **ATLAS** Collaboration, A. R. Martínez, "The Run-2 ATLAS Trigger System," *J. Phys. Conf. Ser.* **762** no. 1, (2016) 012003.

[123] **ATLAS Collaboration** Collaboration, *ATLAS level-1 trigger: Technical Design Report*. Technical Design Report ATLAS. CERN, Geneva, 1998. https://cds.cern.ch/record/381429.

[124] **ATLAS Collaboration** Collaboration, P. Jenni, M. Nessi, M. Nordberg, and K. Smith, *ATLAS high-level trigger, data-acquisition and controls: Technical Design Report*. Technical Design Report ATLAS. CERN, Geneva, 2003. https://cds.cern.ch/record/616089.

[125] **ATLAS** Collaboration, G. Aad *et al.*, "The ATLAS Simulation Infrastructure," *Eur. Phys. J. C* **70** (2010) 823–874, arXiv:1005.4568 [physics.ins-det].

[126] T. Gleisberg, S. Hoeche, F. Krauss, M. Schonherr, S. Schumann, F. Siegert, and J. Winter, "Event generation with SHERPA 1.1," *JHEP* **02** (2009) 007, arXiv:0811.4622 [hep-ph].

[127] A. Buckley *et al.*, "General-purpose event generators for LHC physics," *Phys. Rept.* **504** (2011) 145–233, arXiv:1101.2599 [hep-ph].

[128] V. N. Gribov and L. N. Lipatov, "Deep inelastic e p scattering in perturbation theory," *Sov. J. Nucl. Phys.* **15** (1972) 438–450.

[129] J. Blumlein, T. Doyle, F. Hautmann, M. Klein, and A. Vogt, "Structure functions in deep inelastic scattering at HERA," in *Workshop on Future Physics at HERA (To be followed by meetings 7-9 Feb and 30-31 May 1996 at DESY)*. 9, 1996. arXiv:hep-ph/9609425.

[130] A. Buckley, J. Ferrando, S. Lloyd, K. Nordström, B. Page, M. Rüfenacht, M. Schönherr, and G. Watt, "LHAPDF6: parton density access in the LHC precision era," *Eur. Phys. J. C* **75** (2015) 132, arXiv:1412.7420 [hep-ph].

[131] M. Bengtsson and T. Sjostrand, "Coherent Parton Showers Versus Matrix Elements: Implications of PETRA - PEP Data," *Phys. Lett. B* **185** (1987) 435.

[132] S. Catani, F. Krauss, R. Kuhn, and B. R. Webber, "QCD matrix elements + parton showers," *JHEP* **11** (2001) 063, arXiv:hep-ph/0109231.

[133] L. Lonnblad, "Correcting the color dipole cascade model with fixed order matrix elements," *JHEP* **05** (2002) 046, arXiv:hep-ph/0112284.

[134] B. Andersson, G. Gustafson, G. Ingelman, and T. Sjostrand, "Parton Fragmentation and String Dynamics," *Phys. Rept.* **97** (1983) 31–145.

[135] B. Andersson, *The Lund Model*. Cambridge Monographs on Particle Physics, Nuclear Physics and Cosmology. Cambridge University Press, 1998.

[136] D. Amati and G. Veneziano, "Preconfinement as a Property of Perturbative QCD," *Phys. Lett. B* **83** (1979) 87–92.

[137] M. Dobbs and J. B. Hansen, "The HepMC C++ Monte Carlo event record for High Energy Physics," *Comput. Phys. Commun.* **134** (2001) 41–46.

[138] **GEANT4** Collaboration, S. Agostinelli *et al.*, "GEANT4: A Simulation toolkit," *Nucl. Instrum. Meth.* **A506** (2003) 250–303.

[139] **ATLAS Collaboration** Collaboration, "The new Fast Calorimeter Simulation in ATLAS," Tech. Rep. ATL-SOFT-PUB-2018-002, CERN, Geneva, Jul, 2018. https://cds.cern.ch/record/2630434.

[140] K. Cranmer, "Practical Statistics for the LHC," in *2011 European School of High-Energy Physics*, pp. 267–308. 2014. arXiv:1503.07622 [physics.data-an].

[141] G. Cowan, K. Cranmer, E. Gross, and O. Vitells, "Asymptotic formulae for likelihood-based tests of new physics," *Eur. Phys. J.* **C71** (2011) 1554, arXiv:1007.1727 [physics.data-an]. [Erratum: Eur. Phys. J.C73,2501(2013)].

[142] ATLAS Collaboration, "Reproduction searches for new physics with the ATLAS experiment through publication of full statistical likelihoods." ATL-PHYS-PUB-2019-029, 2019. https://cds.cern.ch/record/2684863.

[143] **ROOT Collaboration** Collaboration, K. Cranmer, G. Lewis, L. Moneta, A. Shibata, and W. Verkerke, "HistFactory: A tool for creating statistical models for use with RooFit and RooStats," Tech. Rep. CERN-OPEN-2012-016, New York U., New York, Jan, 2012. https://cds.cern.ch/record/1456844.

[144] A. Wald, "Tests of statistical hypotheses concerning several parameters when the number of observations is large," *Transactions of the American Mathematical Society* **54** no. 3, (1943) 426–482. https://doi.org/10.1090/S0002-9947-1943-0012401-3.

[145] S. S. Wilks, "The large-sample distribution of the likelihood ratio for testing composite hypotheses," *Ann. Math. Statist.* **9** no. 1, (03, 1938) 60–62. https://doi.org/10.1214/aoms/1177732360.

[146] G. Cowan, "Statistics for Searches at the LHC," in *69th Scottish Universities Summer School in Physics: LHC Physics*, pp. 321–355. 7, 2013. arXiv:1307.2487 [hep-ex].

[147] A. L. Read, "Presentation of search results: the CL_S technique," *J. Phys. G* **28** (2002) 2693.

[148] R. D. Cousins, J. T. Linnemann, and J. Tucker, "Evaluation of three methods for calculating statistical significance when incorporating a systematic uncertainty into a test of the background-only hypothesis for a Poisson process," *Nucl. Instrum. Meth. A* **595** no. 2, (2008) 480, arXiv:physics/0702156 [physics.data-an].

[149] K. CRANMER, "Statistical challenges for searches for new physics at the lhc," *Statistical Problems in Particle Physics, Astrophysics and Cosmology* (May, 2006) . http://dx.doi.org/10.1142/9781860948985_0026.

[150] ATLAS Collaboration, "Search for direct pair production of a chargino and a neutralino decaying to the 125 GeV Higgs boson in $\sqrt{s} = 8$ TeV pp collisions with the ATLAS detector," *Eur. Phys. J. C* **75** (2015) 208, arXiv:1501.07110 [hep-ex].

[151] ATLAS Collaboration, "Search for chargino and neutralino production in final states with a Higgs boson and missing transverse momentum at $\sqrt{s} = 13$ TeV with the ATLAS detector," *Phys. Rev. D* **100** (2019) 012006, arXiv:1812.09432 [hep-ex].

[152] CMS Collaboration, "Search for electroweak production of charginos and neutralinos in WH events in proton–proton collisions at $\sqrt{s} = 13\,\text{TeV}$," *JHEP* **11** (2017) 029, arXiv:1706.09933 [hep-ex].

[153] ATLAS Collaboration, "Search for direct production of electroweakinos in final states with one lepton, missing transverse momentum and a Higgs boson decaying into two b-jets in pp collisions at $\sqrt{s} = 13\,\text{TeV}$ with the ATLAS detector," *Eur. Phys. J. C* **80** (2020) 691, arXiv:1909.09226 [hep-ex].

[154] ATLAS Collaboration, "Improvements in $t\bar{t}$ modelling using NLO+PS Monte Carlo generators for Run 2." ATL-PHYS-PUB-2018-009, 2018. https://cds.cern.ch/record/2630327.

[155] ATLAS Collaboration, "Modelling of the $t\bar{t}H$ and $t\bar{t}V(V = W, Z)$ processes for $\sqrt{s} = 13$ TeV ATLAS analyses." ATL-PHYS-PUB-2016-005, 2016. https://cds.cern.ch/record/2120826.

[156] ATLAS Collaboration, "ATLAS simulation of boson plus jets processes in Run 2." ATL-PHYS-PUB-2017-006, 2017. https://cds.cern.ch/record/2261937.

[157] ATLAS Collaboration, "Multi-Boson Simulation for 13 TeV ATLAS Analyses." ATL-PHYS-PUB-2017-005, 2017. https://cds.cern.ch/record/2261933.

[158] ATLAS Collaboration, "Multi-boson simulation for 13 TeV ATLAS analyses." ATL-PHYS-PUB-2016-002, 2016. https://cds.cern.ch/record/2119986.

[159] J. Alwall, R. Frederix, S. Frixione, V. Hirschi, F. Maltoni, O. Mattelaer, H. S. Shao, T. Stelzer, P. Torrielli, and M. Zaro, "The automated computation of tree-level and next-to-leading order differential cross sections, and their matching to parton shower simulations," *JHEP* **07** (2014) 079, arXiv:1405.0301 [hep-ph].

[160] R. Frederix and S. Frixione, "Merging meets matching in MC@NLO," *JHEP* **12** (2012) 061, arXiv:1209.6215 [hep-ph].

[161] T. Sjöstrand, S. Ask, J. R. Christiansen, R. Corke, N. Desai, P. Ilten, S. Mrenna, S. Prestel, C. O. Rasmussen, and P. Z. Skands, "An Introduction to PYTHIA 8.2," *Comput. Phys. Commun.* **191** (2015) 159–177, arXiv:1410.3012 [hep-ph].

[162] L. Lönnblad and S. Prestel, "Matching tree-level matrix elements with interleaved showers," *JHEP* **03** (2012) 019, arXiv:1109.4829 [hep-ph].

[163] R. D. Ball *et al.*, "Parton distributions with LHC data," *Nucl. Phys. B* **867** (2013) 244, arXiv:1207.1303 [hep-ph].

[164] ATLAS Collaboration, "ATLAS Pythia 8 tunes to 7 TeV data." ATL-PHYS-PUB-2014-021, 2014. https://cds.cern.ch/record/1966419.

[165] D. J. Lange, "The EvtGen particle decay simulation package," *Nucl. Instrum. Meth. A* **462** (2001) 152.

[166] ATLAS Collaboration, "The Pythia 8 A3 tune description of ATLAS minimum bias and inelastic measurements incorporating the Donnachie–Landshoff diffractive model." ATL-PHYS-PUB-2016-017, 2016. https://cds.cern.ch/record/2206965.

[167] B. Fuks, M. Klasen, D. R. Lamprea, and M. Rothering, "Precision predictions for electroweak superpartner production at hadron colliders with RESUMMINO," *Eur. Phys. J. C* **73** (2013) 2480, arXiv:1304.0790 [hep-ph].

[168] J. Fiaschi and M. Klasen, "Neutralino-chargino pair production at NLO+NLL with resummation-improved parton density functions for LHC Run II," *Phys. Rev. D* **98** no. 5, (2018) 055014, arXiv:1805.11322 [hep-ph].

[169] B. Fuks, M. Klasen, D. R. Lamprea, and M. Rothering, "Gaugino production in proton-proton collisions at a center-of-mass energy of 8 TeV," *JHEP* **10** (2012) 081, arXiv:1207.2159 [hep-ph].

[170] S. Alioli, P. Nason, C. Oleari, and E. Re, "A general framework for implementing NLO calculations in shower Monte Carlo programs: the POWHEG BOX," *JHEP* **06** (2010) 043, arXiv:1002.2581 [hep-ph].

[171] S. Frixione, P. Nason, and G. Ridolfi, "A Positive-weight next-to-leading-order Monte Carlo for heavy flavour hadroproduction," *JHEP* **09** (2007) 126, arXiv:0707.3088 [hep-ph].

[172] P. Nason, "A New method for combining NLO QCD with shower Monte Carlo algorithms," *JHEP* **11** (2004) 040, arXiv:hep-ph/0409146.

[173] E. Bothmann *et al.*, "Event generation with Sherpa 2.2," *SciPost Phys.* **7** no. 3, (2019) 034, arXiv:1905.09127 [hep-ph].

[174] S. Höche, F. Krauss, S. Schumann, and F. Siegert, "QCD matrix elements and truncated showers," *JHEP* **05** (2009) 053, arXiv:0903.1219 [hep-ph].

[175] S. Höche, F. Krauss, M. Schönherr, and F. Siegert, "QCD matrix elements + parton showers. The NLO case," *JHEP* **04** (2013) 027, arXiv:1207.5030 [hep-ph].

[176] **NNPDF** Collaboration, R. D. Ball *et al.*, "Parton distributions for the LHC run II," *JHEP* **04** (2015) 040, arXiv:1410.8849 [hep-ph].

[177] ATLAS Collaboration, "Example ATLAS tunes of Pythia8, Pythia6 and Powheg to an observable sensitive to Z boson transverse momentum." ATL-PHYS-PUB-2013-017, 2013. https://cds.cern.ch/record/1629317.

[178] M. Czakon and A. Mitov, "Top++: A program for the calculation of the top-pair cross-section at hadron colliders," *Comput. Phys. Commun.* **185** (2014) 2930, arXiv:1112.5675 [hep-ph].

[179] M. Cacciari, M. Czakon, M. Mangano, A. Mitov, and P. Nason, "Top-pair production at hadron colliders with next-to-next-to-leading logarithmic soft-gluon resummation," *Phys. Lett. B* **710** (2012) 612–622, arXiv:1111.5869 [hep-ph].

[180] P. Kant, O. M. Kind, T. Kintscher, T. Lohse, T. Martini, S. Mölbitz, P. Rieck, and P. Uwer, "HatHor for single top-quark production: Updated predictions and uncertainty estimates for single top-quark production in hadronic collisions," *Comput. Phys. Commun.* **191** (2015) 74–89, arXiv:1406.4403 [hep-ph].

[181] N. Kidonakis, "Two-loop soft anomalous dimensions for single top quark associated production with a W^- or H^-," *Phys. Rev. D* **82** (2010) 054018, arXiv:1005.4451 [hep-ph].

[182] J. M. Campbell and R. K. Ellis, "$t\bar{t}W^{+-}$ production and decay at NLO," *JHEP* **07** (2012) 052, arXiv:1204.5678 [hep-ph].

[183] A. Lazopoulos, T. McElmurry, K. Melnikov, and F. Petriello, "Next-to-leading order QCD corrections to $t\bar{t}Z$ production at the LHC," *Phys. Lett. B* **666** (2008) 62–65, arXiv:0804.2220 [hep-ph].

[184] R. Gavin, Y. Li, F. Petriello, and S. Quackenbush, "FEWZ 2.0: A code for hadronic Z production at next-to-next-to-leading order," arXiv:1011.3540 [hep-ph].

[185] **LHC Higgs Cross Section Working Group** Collaboration, D. de Florian *et al.*, "Handbook of LHC Higgs Cross Sections: 4. Deciphering the Nature of the Higgs Sector," arXiv:1610.07922 [hep-ph].

[186] ATLAS Collaboration, "Performance of the ATLAS track reconstruction algorithms in dense environments in LHC Run 2," *Eur. Phys. J. C* **77** (2017) 673, arXiv:1704.07983 [hep-ex].

[187] R. Frühwirth, "Application of Kalman filtering to track and vertex fitting," *Nucl. Instrum. Methods Phys. Res., A* **262** no. HEPHY-PUB-503, (Jun, 1987) 444. 19 p. https://cds.cern.ch/record/178627.

[188] T. Cornelissen, M. Elsing, I. Gavrilenko, W. Liebig, E. Moyse, and A. Salzburger, "The new ATLAS track reconstruction (NEWT)," *J. Phys.: Conf. Ser.* **119** (2008) 032014. https://cds.cern.ch/record/1176900.

[189] ATLAS Collaboration, "Vertex Reconstruction Performance of the ATLAS Detector at $\sqrt{s} = 13$ TeV." ATL-PHYS-PUB-2015-026, 2015. https://cds.cern.ch/record/2037717.

[190] ATLAS Collaboration, "Reconstruction of primary vertices at the ATLAS experiment in Run 1 proton–proton collisions at the LHC," *Eur. Phys. J. C* **77** (2017) 332, arXiv:1611.10235 [hep-ex].

[191] ATLAS Collaboration, "Topological cell clustering in the ATLAS calorimeters and its performance in LHC Run 1," *Eur. Phys. J. C* **77** (2017) 490, arXiv:1603.02934 [hep-ex].

[192] ATLAS Collaboration, "Electron and photon performance measurements with the ATLAS detector using the 2015–2017 LHC proton–proton collision data," *JINST* **14** (2019) P12006, arXiv:1908.00005 [hep-ex].

[193] ATLAS Collaboration, "Measurement of the photon identification efficiencies with the ATLAS detector using LHC Run 2 data collected in 2015 and 2016," *Eur. Phys. J. C* **79** (2019) 205, arXiv:1810.05087 [hep-ex].

[194] ATLAS Collaboration, "Electron and photon energy calibration with the ATLAS detector using 2015–2016 LHC proton–proton collision data," *JINST* **14** (2019) P03017, arXiv:1812.03848 [hep-ex].

[195] ATLAS Collaboration, "Electron reconstruction and identification in the ATLAS experiment using the 2015 and 2016 LHC proton–proton collision data at $\sqrt{s} = 13$ TeV," *Eur. Phys. J. C* **79** (2019) 639, arXiv:1902.04655 [hep-ex].

[196] ATLAS Collaboration, "Muon reconstruction performance of the ATLAS detector in proton–proton collision data at $\sqrt{s} = 13$ TeV," *Eur. Phys. J. C* **76** (2016) 292, arXiv:1603.05598 [hep-ex].

[197] **ATLAS** Collaboration, "Muon reconstruction and identification efficiency in ATLAS using the full Run 2 pp collision data set at $\sqrt{s} = 13$ TeV," arXiv:2012.00578 [hep-ex].

[198] M. Cacciari, G. P. Salam, and G. Soyez, "The anti-k_t jet clustering algorithm," *JHEP* **04** (2008) 063, arXiv:0802.1189 [hep-ph].

[199] M. Cacciari, G. P. Salam, and G. Soyez, "FastJet user manual," *Eur. Phys. J. C* **72** (2012) 1896, arXiv:1111.6097 [hep-ph].

[200] M. Cacciari, "FastJet: A Code for fast k_t clustering, and more," in *Deep inelastic scattering. Proceedings, 14th International Workshop, DIS 2006, Tsukuba, Japan, April 20-24, 2006*, pp. 487–490. 2006. arXiv:hep-ph/0607071 [hep-ph]. [,125(2006)].

[201] **ATLAS** Collaboration, G. Aad *et al.*, "Jet energy scale and resolution measured in proton-proton collisions at $\sqrt{s} = 13$ TeV with the ATLAS detector," arXiv:2007.02645 [hep-ex].

[202] M. Cacciari and G. P. Salam, "Pileup subtraction using jet areas," *Phys. Lett. B* **659** (2008) 119–126, arXiv:0707.1378 [hep-ph].

[203] ATLAS Collaboration, "Jet energy measurement with the ATLAS detector in proton–proton collisions at $\sqrt{s} = 7$ TeV," *Eur. Phys. J. C* **73** (2013) 2304, arXiv:1112.6426 [hep-ex].

[204] ATLAS Collaboration, "Determination of jet calibration and energy resolution in proton–proton collisions at $\sqrt{s} = 8$ TeV using the ATLAS detector," arXiv:1910.04482 [hep-ex].

[205] ATLAS Collaboration, "Performance of pile-up mitigation techniques for jets in pp collisions at $\sqrt{s} = 8$ TeV using the ATLAS detector," *Eur. Phys. J. C* **76** (2016) 581, arXiv:1510.03823 [hep-ex].

[206] ATLAS Collaboration, "Optimisation and performance studies of the ATLAS b-tagging algorithms for the 2017-18 LHC run." ATL-PHYS-PUB-2017-013, 2017. https://cds.cern.ch/record/2273281.

[207] ATLAS Collaboration, "ATLAS b-jet identification performance and efficiency measurement with $t\bar{t}$ events in pp collisions at $\sqrt{s} = 13$ TeV," *Eur. Phys. J. C* **79** (2019) 970, arXiv:1907.05120 [hep-ex].

[208] ATLAS Collaboration, "Measurements of b-jet tagging efficiency with the ATLAS detector using $t\bar{t}$ events at $\sqrt{s} = 13$ TeV," *JHEP* **08** (2018) 089, arXiv:1805.01845 [hep-ex].

[209] ATLAS Collaboration, "Performance of missing transverse momentum reconstruction with the ATLAS detector using proton–proton collisions at $\sqrt{s} = 13$ TeV," *Eur. Phys. J. C* **78** (2018) 903, arXiv:1802.08168 [hep-ex].

[210] **ATLAS Collaboration** Collaboration, "$E_{\mathrm{T}}^{\mathrm{miss}}$ performance in the ATLAS detector using 2015-2016 LHC p-p collisions," Tech. Rep. ATLAS-CONF-2018-023, CERN, Geneva, Jun, 2018. http://cds.cern.ch/record/2625233.

[211] D. Adams *et al.*, "Recommendations of the Physics Objects and Analysis Harmonisation Study Groups 2014," Tech. Rep. ATL-PHYS-INT-2014-018, CERN, Geneva, Jul, 2014. https://cds.cern.ch/record/1743654.

[212] M. Cacciari, G. P. Salam, and G. Soyez, "The Catchment Area of Jets," *JHEP* **04** (2008) 005, arXiv:0802.1188 [hep-ph].

[213] **UA1** Collaboration, G. Arnison *et al.*, "Experimental Observation of Isolated Large Transverse Energy Electrons with Associated Missing Energy at $\sqrt{s} = 540$ GeV," *Phys. Lett. B* **122** (1983) 103–116.

[214] **Aachen-Annecy-Birmingham-CERN-Helsinki-London(QMC)-Paris(CdF)-Riverside-Rome-Rutherford-Saclay(CEN)-Vienna** Collaboration, G. Arnison *et al.*, "Further evidence for charged intermediate vector bosons at the SPS collider," *Phys. Lett. B* **129** no. CERN-EP-83-111, (Jun, 1985) 273–282. 17 p. https://cds.cern.ch/record/163856.

[215] D. R. Tovey, "On measuring the masses of pair-produced semi-invisibly decaying particles at hadron colliders," *JHEP* **04** (2008) 034, arXiv:0802.2879 [hep-ph].

[216] G. Polesello and D. R. Tovey, "Supersymmetric particle mass measurement with the boost-corrected contransverse mass," *JHEP* **03** (2010) 030, arXiv:0910.0174 [hep-ph].

[217] **ATLAS** Collaboration, G. Aad *et al.*, "Performance of the missing transverse momentum triggers for the ATLAS detector during Run-2 data taking," *JHEP* **08** (2020) 080, arXiv:2005.09554 [hep-ex].

[218] **ATLAS** Collaboration, G. Aad *et al.*, "Performance of algorithms that reconstruct missing transverse momentum in $\sqrt{s} = 8$ TeV proton-proton collisions in the ATLAS detector," *Eur. Phys. J. C* **77** no. 4, (2017) 241, arXiv:1609.09324 [hep-ex].

[219] ATLAS Collaboration, "ATLAS data quality operations and performance for 2015–2018 data-taking," *JINST* **15** (2020) P04003, arXiv:1911.04632 [physics.ins-det].

[220] ATLAS Collaboration, "Selection of jets produced in 13 TeV proton–proton collisions with the ATLAS detector." ATLAS-CONF-2015-029, 2015. https://cds.cern.ch/record/2037702.

[221] N. Hartmann, "ahoi." https://gitlab.com/nikoladze/ahoi, 2018.

[222] **ATLAS** Collaboration, "Object-based missing transverse momentum significance in the ATLAS detector," Tech. Rep. ATLAS-CONF-2018-038, CERN, Geneva, Jul, 2018. https://cds.cern.ch/record/2630948.